LETTERS

Direct observation of the superfluid phase transition in ultracold Fermi gases

Martin W. Zwierlein[1], Christian H. Schunck[1], André Schirotzek[1] & Wolfgang Ketterle[1]

Phase transitions are dramatic phenomena: water freezes into ice, atomic spins spontaneously align in a magnet, and liquid helium becomes superfluid. Sometimes, such a drastic change in behaviour is accompanied by a visible change in appearance. The hallmark of Bose–Einstein condensation and superfluidity in trapped, weakly interacting Bose gases is the sudden formation of a dense central core inside a thermal cloud[1–7]. However, in strongly interacting gases—such as the recently observed fermionic superfluids[8]—there is no longer a clear separation between the superfluid and the normal parts of the cloud. The detection of fermion pair condensates has required magnetic field sweeps[9–11] into the weakly interacting regime, and the quantitative description of these sweeps presents a major theoretical challenge. Here we report the direct observation of the superfluid phase transition in a strongly interacting gas of ^{6}Li fermions, through sudden changes in the shape of the clouds—in complete analogy to the case of weakly interacting Bose gases. By preparing unequal mixtures of the two spin components involved in the pairing[12,13], we greatly enhance the contrast between the superfluid core and the normal component. Furthermore, the distribution of non-interacting excess atoms serves as a direct and reliable thermometer. Even in the normal state, strong interactions significantly deform the density profile of the majority spin component. We show that it is these interactions that drive the normal-to-superfluid transition at the critical population imbalance of 70 ± 5 per cent (ref. 12).

The dramatic signature of Bose–Einstein condensation in weakly interacting gases in atom traps derives from a natural hierarchy of energy scales: the critical temperature for condensation, $T_C \propto n^{2/3}$ at particle density n, is much larger than the chemical potential (divided by the Boltzmann constant k_B) of a pure condensate, $\mu \propto na$, which measures the interaction strength between particles (a is the scattering length). Hence, for weak (repulsive) interactions ($a > 0$, $na^3 \ll 1$), the condensate is clearly distinguished from the cloud of uncondensed particles through its smaller size and higher density. However, as the interactions are increased, for example by tuning a using a Feshbach resonance, this hierarchy of energy scales breaks down, as μ can now become comparable to $k_B T_C$. In Fermi gases with weak attractive interaction ($a < 0$, $n|a|^3 \ll 1$), the chemical potential is given by the Fermi energy E_F and will even far exceed the superfluid transition temperature $k_B T_C \propto E_F e^{-\pi/2k_F|a|}$ (where $k_F \propto n^{1/3}$ is the Fermi wave vector). Both the normal and the condensed cloud will here be of the same size and shape, dependent only on E_F and the trapping potential.

The phase transition from the normal to the superfluid state, although dramatic in its consequences, is thus not revealed by a major change in the appearance of the gas. Indeed, in strongly interacting Fermi gases no deviation from a normal cloud's shape has so far been detected, either in the unitary regime, where a diverges, or on the attractive Bardeen–Cooper–Schrieffer (BCS) side of a Feshbach resonance. Theoretical works predicted small 'kinks'[14–16] or other slight deviations[17] in the density profiles of the gas in the superfluid regime, but after line-of-sight integration these effects have so far been too small to be observable. Condensates could only be observed via rapid magnetic field ramps to the Bose–Einstein condensate (BEC) side ($a > 0$) of the Feshbach resonance, performed during expansion[9,10]. This suddenly reduced the condensate's chemical potential, and let the thermal fraction grow beyond the condensate size. A similar ramp was used to detect vortices on resonance and on the BCS side in the demonstration of fermionic superfluidity[8]. However, these magnetic field ramps are difficult to model theoretically, and a satisfactory quantitative comparison of, for example, the condensate fraction with experiments has not been accomplished[18–21].

In this work we demonstrate that the normal-to-superfluid phase transition in a strongly interacting Fermi gas can be directly observed in absorption profiles, without the need for any magnetic field ramps. As in the case of weakly interacting BECs, preparation, expansion and detection of the sample all take place at the same, fixed magnetic field and scattering length. As for BECs, the phase transition is observed as a sudden change in the shape of the cloud during time-of-flight expansion, when the trap depth is decreased below a critical value. To clearly distinguish the superfluid from the normal component, we break the number symmetry between spin-up (majority atom number, $N_\uparrow$) and spin-down (minority atom number, $N_\downarrow$) and produce an unequal mixture of fermions (imbalance parameter $\delta = (N_\uparrow - N_\downarrow)/(N_\uparrow + N_\downarrow)$). Standard BCS superfluidity requires equal densities of the two spin components. Hence, when cooled below the phase transition the cloud should show a sudden onset of a superfluid region of equal densities. Indeed, below a critical temperature, we observe how the density distribution of the minority component becomes bimodal.

Breaking the symmetry in atom numbers thus produces a direct and striking signature of the superfluid phase transition[22–24]. A similar situation has been encountered in Bose–Einstein condensation, where breaking the symmetry of a spherical trap resulted in dramatic anisotropic expansion of the condensate, now a hallmark of the BEC phase transition.

Figure 1 shows column density profiles of the two imbalanced spin states for different points along the evaporation path corresponding to different temperatures, and for three magnetic fields that correspond to the BEC side, exact resonance and the BCS side of the resonance. For large final trap depths (upper panels in Fig. 1), the smaller cloud has the expected shape of a normal, non-superfluid gas: it is very well fitted using a single, finite temperature Thomas–Fermi-profile (with central optical density, radius and the fugacity as independent fit-parameters). However, below a critical trap depth, a second, denser feature appears in the centre of the minority component (lower panels in Fig. 1). This onset of bimodality occurs very suddenly as the trap depth is lowered, as can be seen from Fig. 2: Around the critical point, the atom number (Fig. 2a) and population

[1]Department of Physics, MIT-Harvard Center for Ultracold Atoms, and Research Laboratory of Electronics, MIT, Cambridge, Massachusetts 02139, USA.

imbalance (Fig. 2b) are practically constant, and the temperature (Fig. 2c) varies in a smooth linear way with the trap depth. In contrast, below the critical trap depth, the shape of the smaller cloud starts to deviate drastically from the Thomas–Fermi distribution of a normal gas, as quantified in Fig. 2d. This sudden increase in the standard deviation of a fit to a single-component fitting function is a standard way of identifying the BEC phase transition in a model-independent way[2].

Figure 2e displays the fact that below the critical trap depth a new, third radius is required to describe the two clouds. As we will see below, the appearance of this central feature coincides with the appearance of the fermion pair condensate in experiments involving the magnetic field ramp technique[10–12]. It is this condensate that contains the superfluid vortices in refs 8 and 12. We are thus naturally led to interpret the central core as the condensate of fermion pairs, and the outer wings as the normal, uncondensed part of the cloud. This constitutes, to our knowledge, the first direct observation of the normal-to-superfluid phase transition in resonantly interacting Fermi gases on resonance and on the BCS side (that is, without a magnetic field sweep that so far cannot be quantitatively accounted for).

Already at high temperatures, above the phase transition, the larger cloud's profile is strongly deformed in the presence of the smaller cloud, a direct signature of interaction. Indeed, on resonance the cloud size of the minority component is significantly smaller than that of a non-interacting sample with the same number of atoms (see Fig. 2e). At the phase transition, the outer radii of the clouds do not change abruptly. This demonstrates that interactions, not superfluidity, are the main mechanism behind the reduced cloud size of an interacting Fermi gas.

On the BEC side, the condensate is clearly visible in the larger cloud. On resonance, however, the condensate is not easily discernible in the larger component's profiles at the scale of Fig. 1. Nevertheless, we have found a very faint but reproducible trace of the condensate when analysing the curvature of these column density profiles (see Supplementary Fig. S1). On resonance and on the BCS side, the onset of bimodality in the smaller cloud can be clearly observed for imbalances larger than ~20% (but below a certain critical imbalance, see below), for which the condensate is small compared to the minority cloud size. With increasing magnetic field on the BCS side (that is, with decreasing interaction strength), the bimodality becomes less pronounced and is not clearly discerned beyond 853 G (interaction parameter $1/k_F a < -0.15$).

Thermometry of strongly interacting Fermi gases has always been a major difficulty in experiments on strongly interacting fermions[25]. A thermometer can only be reliable if the working substance is not affected by the sample to be measured. In equal mixtures of fermions, the two overlapping atomic clouds are strongly interacting throughout. Temperatures determined from a non-interacting Thomas–Fermi fit to these clouds need calibration based on approximate theoretical calculations[25]. In addition, as will be reported elsewhere, we find that those fits do not describe the profiles of a partially superfluid Fermi gas as well as they do in the normal state, in agreement with theory[14–17]. In the case of imbalanced mixtures, the wings of the larger component, where the spin-down species are absent, are non-interacting and thus serve as a direct thermometer (see Fig. 2c). For an imbalance of $\delta = 75 \pm 3\%$ we determine the critical temperature for the phase transition on the BEC side at $1/k_F a = 0.46$ to be $T/T_F = 0.18(3)$ ($k_B T_F = \hbar\omega(3(N_\uparrow + N_\downarrow))^{1/3} \equiv \hbar^2 k_F^2/2m$ is the Fermi energy of a non-interacting, equal mixture with the same total number of fermions $N_\uparrow + N_\downarrow$, $\omega/2\pi$ is the

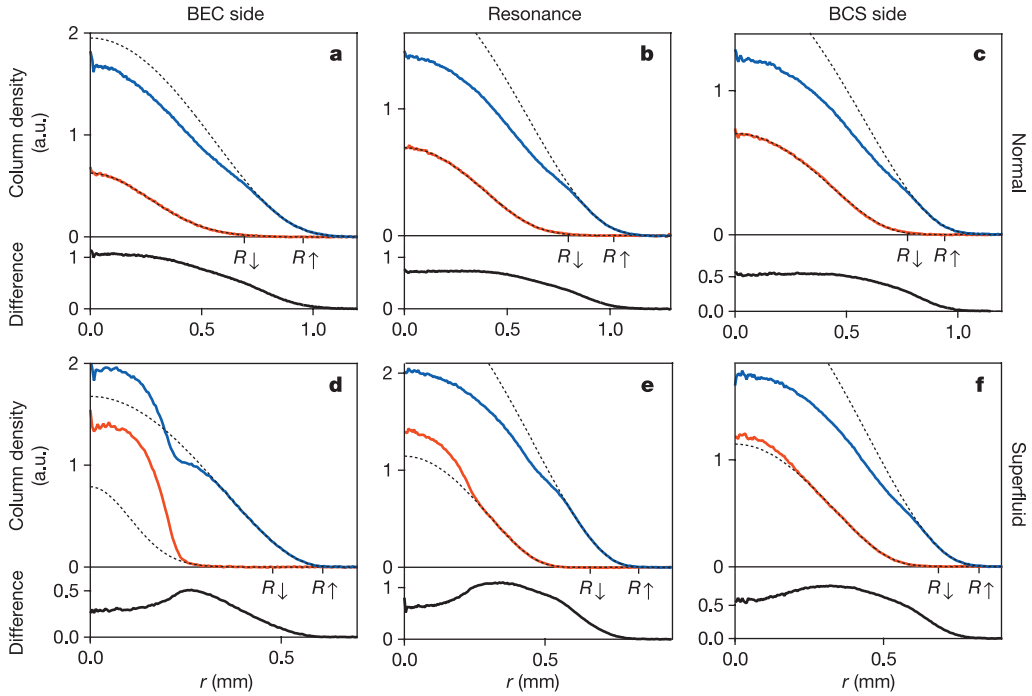

Figure 1 | Direct observation of the phase transition in a strongly interacting two-state mixture of fermions with imbalanced spin populations. Top (**a**–**c**) and bottom (**d**–**f**) rows show the normal and the superfluid state, respectively. Panels **a** and **d** were obtained in the BEC regime (at $B = 781$ G), **b** and **e** on resonance (834 G), and **c** and **f** on the BCS side of the Feshbach resonance (853 G). The profiles represent the azimuthal average of the column density after 10 ms (BEC side) or 11 ms (on resonance and BCS side) of expansion. The appearance of a dense central feature in the smaller component marks the onset of condensation. The condensate causes a clear depletion in the difference profiles (bottom of each panel). Both in the normal and in the superfluid state, interactions between the two spin states are manifest in the strong deformation of the larger component. The dotted lines show Thomas–Fermi fits to the wings of the column density. The radii $R_\uparrow$ and $R_\downarrow$ mark the Fermi radius of a ballistically expanding, non-interacting cloud with atom number $N_\uparrow$, $N_\downarrow$. The trap depth U (in μK), the atom numbers, the population imbalance δ (in %), the interaction parameter $1/k_F a$, the temperature T (in nK) and the reduced temperature T/T_F were respectively: **a**, 4.8, 1.8×10^7 and 2.6×10^6, 75, 0.42, 350, 0.20; **b**, 3.2, 1.8×10^7 and 4.2×10^6, 63, 0 (resonance), 260, 0.15; **c**, 2.5, 1.5×10^7 and 4.5×10^6, 52, −0.13, 190, 0.12; **d**, 0.8, 6.5×10^6 and 1.5×10^6, 62, 0.67, 50, ≤0.05; **e**, 1.1, 1.5×10^7 and 3.8×10^6, 60%, 0 (resonance), 70, 0.06; **f**, 1.2, 1.3×10^7 and 4.4×10^6, 50, −0.15, 100, 0.08. a.u., arbitrary units.

geometric mean of the trapping frequencies, and m is the mass of ^{6}Li). This corresponds to $T/T_{C,\downarrow} = 0.55(9)$ when comparing the temperature to the critical temperature $T_{C,\downarrow}$ for Bose condensation in a non-interacting gas with $N_\downarrow$ bosons. The reduction in the critical temperature is a direct consequence of strong repulsive interactions between the molecules. On resonance, at $\delta = 59 \pm 3\%$, we find $T/T_F = 0.12(2)$, and on the BCS side ($1/k_F a = -0.14$) for $\delta = 53 \pm 3\%$ we obtain $T/T_F = 0.11(2)$. These are, to our knowledge, the first directly measured and reliable temperatures for the superfluid transition in strongly interacting Fermi gases. They may serve as a checkpoint for theoretical models.

We note that the critical temperature will in general depend on the population imbalance. For example, for large enough imbalance on resonance or on the BCS side, no condensate will form even at zero temperature[12], as we discuss below. Here, the critical temperature for superfluidity will be zero.

An important qualitative difference distinguishes the BEC side from resonance at the lowest temperatures. On the BEC side, the gas consists of only two parts—the superfluid core surrounded by a fully polarized degenerate Fermi gas of the excess species. On resonance and on the BCS side, however, there exists a third region, a normal state in which both species are mixed. Several recent theories describe

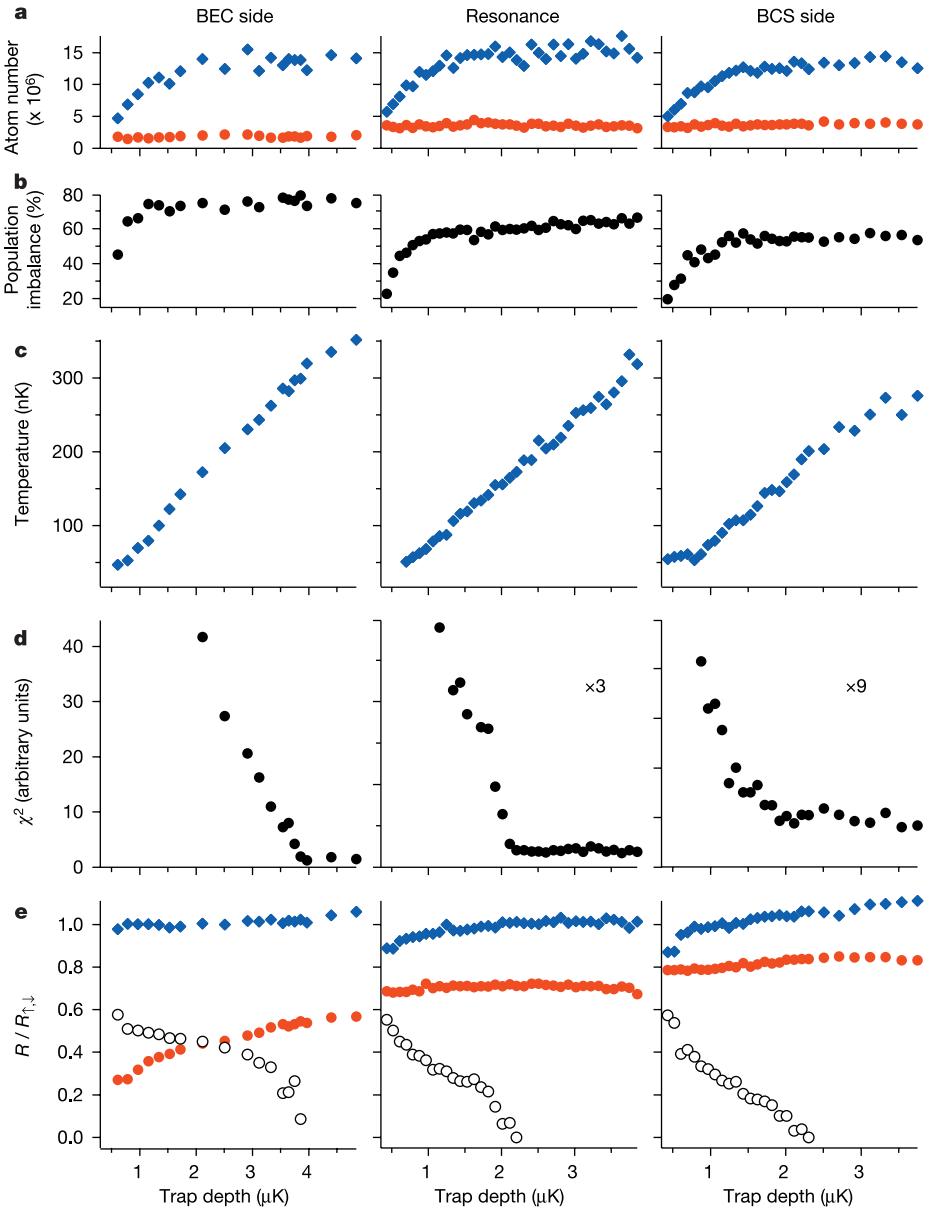

Figure 2 | Characterization of the phase transition. a–e, The data characterize the evolution of the fermion mixture as the cloud is evaporatively cooled by lowering the trap depth. The chosen magnetic fields are identical to those in Fig. 1. Data obtained from the majority (minority) cloud are shown as diamonds (circles). **a**, The atom number; **b**, the population imbalance between the two spin states; and **c**, the temperature of the spin mixture as determined from the non-interacting wings of the larger cloud's profile. **d**, A finite temperature Fermi–Dirac (for resonance and the BCS side) or gaussian (for the BEC side) distribution is fitted to the minority cloud; the phase transition is marked by a sudden increase in χ^2 as the condensate starts to appear. **e**, Outer radii of the majority and minority cloud (for the minority cloud on the BEC side, thermal cloud radius; all other cases, Thomas–Fermi radius) as well as the condensate radius (open circles), defined as the position of the 'kink' in the minority profile (see Fig. 1). The majority (minority and condensate) cloud size is normalized by the Fermi radius $R_\uparrow$ ($R_\downarrow$) of a non-interacting cloud with $N_\uparrow$ ($N_\downarrow$) atoms, and adjusted for ballistic (hydrodynamic) expansion. Note that the imbalance decreases during evaporation because the larger majority cloud incurs stronger evaporative losses. For the data, three (BEC and resonance) to five (BCS) independent measurements were averaged.

density profiles of imbalanced Fermi mixtures[26–32]. Mean-field theories that neglect interactions in the normal cloud and between the normal and condensed cloud are only in qualitative agreement with our results. Descriptions that exclude the mixed region or find superfluidity on resonance at all population imbalances are ruled out by our observations.

To elucidate the origin of the clear separation between condensate and normal components, we varied the population imbalance at our coldest temperatures and on resonance. Figure 3b shows several resulting profiles after 11 ms expansion from the trap. For large imbalances, $\delta > 70\%$, the minority cloud is not bimodal and well fitted by a (unconstrained) Thomas–Fermi profile. At a critical imbalance of $\delta \approx 70\%$, the condensate appears and then grows further as the imbalance is reduced (for the cloud radii, see Supplementary Fig. S2).

To characterize the appearance of the condensate for imbalances around $\delta = 70\%$, a Thomas–Fermi profile is fitted to the wings of the minority cloud. The fraction of atoms not contained in this fit is a measure of the condensate fraction (see Fig. 3). We find a critical imbalance of $\delta_c = 70(5)\%$ above which the condensate disappears. This agrees with our previous work[12], where we employed a rapid ramp method to the BEC side to extract the condensate fraction. We

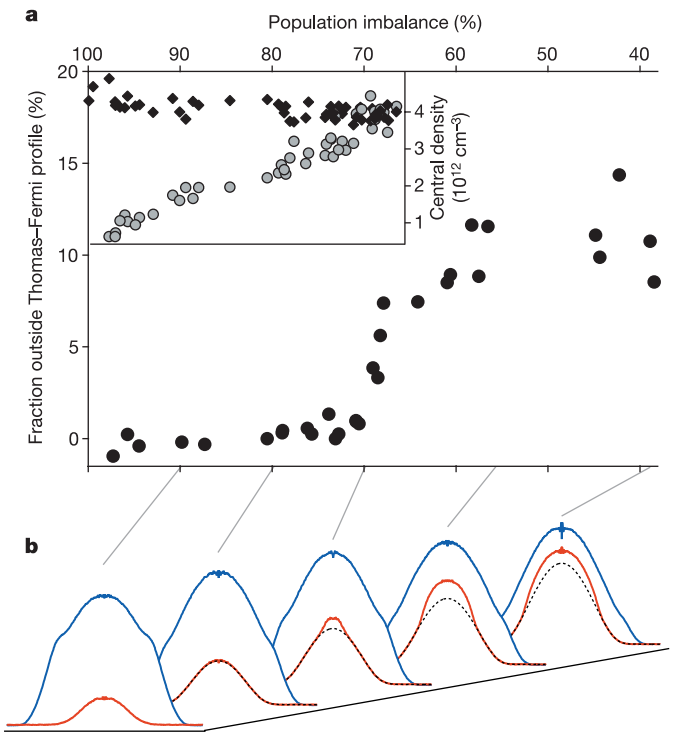

Figure 3 | Quantum phase transition to superfluidity for decreasing population imbalance. **a**, Main panel, the 'condensate fraction' of excess minority atoms, not contained in the Thomas–Fermi fit, versus population imbalance on resonance. **b**, Column density profiles of majority (blue) and minority (red) clouds, azimuthally averaged, for varying population imbalance. The condensate is clearly visible in the minority component as the dense central feature on top of the normal background (finite-temperature Thomas–Fermi fit, dotted lines). Below the critical imbalance $\delta_c = 70\%$, the condensate starts to form. The inset in **a** shows the central densities of the larger (black diamonds) and smaller (grey circles) cloud in the normal state above δ_c. This demonstrates that here the central densities are unequal, suppressing superfluidity. The densities were calculated from the central optical density and the fitted size of the clouds, assuming local density approximation and adjusting for ballistic (hydrodynamic) expansion of the outer radii of majority (minority) clouds. The data points for the condensate fraction show the average of several independent measurements.

observed the quantum phase transition from the superfluid to the normal state as a critical population imbalance of $\delta_c = 70\%$ was exceeded. This strongly suggests that the bimodality observed here directly in the minority component, and the bimodality observed in molecular clouds after a magnetic field sweep, are signatures of the same phase transition.

The transition at δ_c is known as the Clogston limit of superfluidity[12,33], and occurs when the chemical potential difference $\delta\mu$ becomes larger than a constant times the (local) superfluid gap $\Delta(\mathbf{r})$ (see Supplementary Information). Here we present a simple picture for the character of this phase transition in a harmonic trap. Thomas–Fermi fits for the normal clouds beyond δ_c allow a simple estimate of the central three-dimensional density of the gas (with an estimated accuracy of 20% for the relative density difference), shown in the inset of Fig. 3. For large imbalances, we find that the three-dimensional densities differ significantly, as is expected for two weakly interacting Fermi clouds. As the imbalance is reduced towards the critical δ_c, the central densities approach each other and become approximately equal around δ_c. This is a direct consequence of strong interactions in the normal state. In a non-interacting Fermi mixture with an imbalance of δ_c, the central densities would differ by a factor of 2.4.

This observation now offers an intriguing insight into the nature of a fermionic superfluid on resonance or on the BCS side. Already in the normal state above T_C or beyond $\delta = \delta_c$, interactions between the two spin states are strong. Indeed, this is directly seen in the deformation of the majority cloud due to the presence of the minority species (see Figs 1, 3). However, here these interactions are not strong enough to let the central densities of the two clouds become comparable. At the critical imbalance the Clogston criterion $\delta\mu = c\Delta(\mathbf{r} = 0)$ is fulfilled in the centre of the trap (here, c is a constant that equals $\sqrt{2}$ in the BCS limit[33]). For smaller imbalance, a central superfluid region can form: the condensate. Its borders are defined by $\delta\mu < c\Delta(\mathbf{r})$. The simple density estimate in Fig. 3 suggests that in this region, the two clouds will have equal densities, although more refined techniques to measure small density differences have to be developed to finally settle this question. Outside the superfluid region there is still a normal state with unequal densities of minority and majority components. The discontinuity in the clouds' densities at the normal-to-superfluid phase boundary gives rise to the visible kink in the column density profiles. Such a density discontinuity is characteristic of a first-order phase transition.

Interestingly, most of the 'work' needed to build the superfluid state has already been done in the normal component by decreasing the density difference. Consequently, the critical population difference needed to form the superfluid is largely determined by the interactions in the normal gas.

In conclusion, we have observed the normal-to-superfluid phase transition through the direct observation of condensation in an imbalanced Fermi mixture—on the BEC side, on the BCS side, and right on the Feshbach resonance. Unequal mixtures offer a direct method of thermometry by analysing the non-interacting wings of the majority species. Strong interactions are already visible in the normal cloud as marked deformations of the majority profile. It is these interactions in the normal gas that squeeze the two components and eventually, at the critical imbalance, let them reach almost equal densities in the centre, aiding the formation of the superfluid. Our method of direct detection of the condensate is a powerful new tool to characterize the superfluid phase transition. At the current level of precision, the appearance of a condensate after magnetic field sweeps and the direct observation of the central dense core occur together, and indicate the normal-to-superfluid phase transition. An intriguing question is whether further phases are possible, including a more exotic superfluid state with unequal densities. Several theories predict that the Fulde–Ferrell–Larkin–Ovchinnikov state, a superfluid state with oscillating order parameter, should be present for imbalanced spin populations[24,26,28].

METHODS

Experimental procedure. Our experimental setup is described in previous publications[8,12]. A spin-polarized cloud of ^{6}Li fermions is cooled to degeneracy using a combination of laser cooling and sympathetic cooling with sodium atoms in a magnetic trap. After transfer into an optical trap, a variable spin mixture of the lowest two hyperfine states, labelled $|\uparrow\rangle$ and $|\downarrow\rangle$, is prepared at a magnetic bias field of 875 G. Interactions between the two spin states can be freely tuned via a 300-G-wide Feshbach resonance located at $B_0 = 834$ G. At fields below B_0, two-body physics supports a stable molecular bound state (BEC side), while at higher fields (BCS side), no such bound state exists for two isolated atoms. Our trap combines a magnetic saddle potential with a weakly focused (waist $w \approx 120\,\mu$m) infrared laser beam (wavelength $\lambda = 1{,}064$ nm), leading to a harmonic axial confinement with oscillation frequency of $\nu_z = 22.8(0.2)$ Hz and a gaussian radial potential with variable trapping frequency ν_r in the central harmonic region. The trap depth U is related to ν_r and ν_z by:

$$U = \frac{1}{4}m(2\pi\nu_r)^2 w^2\left(1 - \frac{\nu_z^2}{2\nu_r^2}\ln\left(\frac{2\left(\nu_r^2 + \nu_z^2/2\right)}{\nu_z^2}\right)\right).$$

The initial degeneracy of the spin mixture is about $T/T_F \approx 0.3$. The strongly interacting gas is further cooled by decreasing the laser power of the optical trap over several seconds and evaporating the most energetic particles. During the first few seconds, the magnetic field is adiabatically ramped to a chosen final field in the resonance region where the last stage of the evaporation (shown in Fig. 2) takes place. For detection, the optical trap is switched off and the gas expands in the remaining magnetic saddle-point potential. After a variable time-of-flight, an absorption image of atoms either in state $|\uparrow\rangle$ or $|\downarrow\rangle$ is taken along the axial direction of the trap (the direction of the optical trapping beam). The cloud's radial symmetry allows for azimuthal averaging of the resulting column densities, leading to low-noise profiles[12].

For preparing clouds at the coldest temperatures (as shown in Fig. 3) with varying population imbalance, the spin mixture is evaporated down to a trap depth of 1 μK over several seconds on resonance, after which the trap depth is increased again to 1.4 μK for more harmonic confinement (trap frequencies: $\nu_r = 115(10)$ Hz and $\nu_z = 22.8(0.2)$ Hz). The temperature of the gas is determined to be $T/T_F \leq 0.06$ for all $\delta > 15\%$, and appears to smoothly rise to $T/T_F = 0.11$ for an equal mixture, although thermometry in the interacting wings is problematic. The total atom number was 1.5×10^7 and constant to within 15% for all values of δ.

Errors. The error in the critical temperature T_C/T_F for the phase transition is dominated by the uncertainty in the atom number entering the determination of T_F, which we estimate to be 30% (ref. 12). For T_F we use the harmonic approximation for the radially gaussian trapping potential, with the measured trapping frequencies reflecting the average curvature of the gaussian potential. The phase transition is observed above $U = 2\,\mu$K, where anharmonicities contribute only 3% to the error in T_F. Note that anharmonicities do not affect the temperature measurement performed on the majority wings: ballistic expansion of non-interacting atoms reveals their momentum distribution, regardless of the shape of the trap.

Received 6 March; accepted 23 May 2006.

1. Anderson, M. H., Ensher, J. R., Matthews, M. R., Wieman, C. E. & Cornell, E. A. Observation of Bose-Einstein condensation in a dilute atomic vapor. *Science* **269,** 198–201 (1995).
2. Davis, K. B. *et al.* Bose-Einstein condensation in a gas of sodium atoms. *Phys. Rev. Lett.* **75,** 3969–3973 (1995).
3. Greiner, M., Regal, C. A. & Jin, D. S. Emergence of a molecular Bose-Einstein condensate from a Fermi gas. *Nature* **426,** 537–540 (2003).
4. Zwierlein, M. W. *et al.* Observation of Bose-Einstein condensation of molecules. *Phys. Rev. Lett.* **91,** 250401 (2003).
5. Bartenstein, M. *et al.* Crossover from a molecular Bose-Einstein condensate to a degenerate Fermi gas. *Phys. Rev. Lett.* **92,** 120401 (2004).
6. Bourdel, T. *et al.* Experimental study of the BEC-BCS crossover region in lithium 6. *Phys. Rev. Lett.* **93,** 050401 (2004).
7. Partridge, G. B., Strecker, K. E., Kamar, R. I., Jack, M. W. & Hulet, R. G. Molecular probe of pairing in the BEC-BCS crossover. *Phys. Rev. Lett.* **95,** 020404 (2005).
8. Zwierlein, M. W., Abo-Shaeer, J. R., Schirotzek, A., Schunck, C. H. & Ketterle, W. Vortices and superfluidity in a strongly interacting Fermi gas. *Nature* **435,** 1047–1051 (2005).
9. Regal, C. A., Greiner, M. & Jin, D. S. Observation of resonance condensation of fermionic atom pairs. *Phys. Rev. Lett.* **92,** 040403 (2004).
10. Zwierlein, M. W. *et al.* Condensation of pairs of fermionic atoms near a Feshbach resonance. *Phys. Rev. Lett.* **92,** 120403 (2004).
11. Zwierlein, M. W., Schunck, C. H., Stan, C. A., Raupach, S. M. F. & Ketterle, W. Formation dynamics of a fermion pair condensate. *Phys. Rev. Lett.* **94,** 180401 (2005).
12. Zwierlein, M. W., Schirotzek, A., Schunck, C. H. & Ketterle, W. Fermionic superfluidity with imbalanced spin populations. *Science* **311,** 492–496 (2006). Published online 21 December 2005 (doi:10.1126/science.1122318).
13. Partridge, G. B., Li, W., Kamar, R. I., Liao, Y. & Hulet, R. G. Pairing and phase separation in a polarized Fermi gas. *Science* **311,** 503–505 (2006). Published online 21 December 2005 (doi:10.1126/science.1122876).
14. Chiofalo, M. L., Kokkelmans, S. J. J. M. F., Milstein, J. N. & Holland, M. J. Signatures of resonance superfluidity in a quantum Fermi gas. *Phys. Rev. Lett.* **88,** 090402 (2002).
15. Ho, T.-L. Universal thermodynamics of degenerate quantum gases in the unitarity limit. *Phys. Rev. Lett.* **92,** 090402 (2004).
16. Perali, A., Pieri, P., Pisani, L. & Strinati, G. C. BCS-BEC crossover at finite temperature for superfluid trapped Fermi atoms. *Phys. Rev. Lett.* **92,** 220404 (2004).
17. Stajic, J., Chen, Q. & Levin, K. Density profiles of strongly interacting trapped Fermi gases. *Phys. Rev. Lett.* **94,** 060401 (2005).
18. Diener, R. B. & Ho, T.-L. Projecting fermion pair condensates into molecular condensates. Preprint at ⟨http://arxiv.org/cond-mat/0404517⟩ (2004).
19. Perali, A., Pieri, P. & Strinati, G. C. Extracting the condensate density from projection experiments with Fermi gases. *Phys. Rev. Lett.* **95,** 010407 (2005).
20. Altman, E. & Vishwanath, A. Dynamic projection on Feshbach molecules: A probe of pairing and phase fluctuations. *Phys. Rev. Lett.* **95,** 110404 (2005).
21. Chen, Q., Regal, C. A., Greiner, M., Jin, D. S. & Levin, K. Understanding the superfluid phase diagram in trapped Fermi gases. *Phys. Rev. A* **73,** 041603 (2006).
22. Bedaque, P. F., Caldas, H. & Rupak, G. Phase separation in asymmetrical fermion superfluids. *Phys. Rev. Lett.* **91,** 247002 (2003).
23. Caldas, H. Cold asymmetrical fermion superfluids. *Phys. Rev. A* **69,** 063602 (2004).
24. Sheehy, D. E. & Radzihovsky, L. BEC-BCS crossover in "magnetized" Feshbach-resonantly paired superfluids. *Phys. Rev. Lett.* **96,** 060401 (2006).
25. Kinast, J. *et al.* Heat capacity of a strongly-interacting Fermi gas. *Science* **307,** 1296–1299 (2005).
26. Mizushima, T., Machida, K. & Ichioka, M. Direct imaging of spatially modulated superfluid phases in atomic fermion systems. *Phys. Rev. Lett.* **94,** 060404 (2005).
27. Pieri, P. & Strinati, G. C. Trapped fermions with density imbalance in the Bose-Einstein condensate limit. *Phys. Rev. Lett.* **96,** 150404 (2006).
28. Kinnunen, J., Jensen, L. M. & Törmä, P. Strongly interacting Fermi gases with density imbalance. *Phys. Rev. Lett.* **96,** 110403 (2006).
29. De Silva, T. N. & Mueller, E. J. Profiles of near-resonant population-imbalanced trapped Fermi gases. *Phys. Rev. A* **73,** 051602(R) (2006).
30. Yi, W. & Duan, L.-M. Trapped fermions across a Feshbach resonance with population imbalance. *Phys. Rev. A* **73,** 031604(R) (2006).
31. Chevy, F. Density profile of a trapped strongly interacting Fermi gas with unbalanced spin populations. *Phys. Rev. Lett.* **96,** 130401 (2006).
32. Haque, M. & Stoof, H. T. C. Pairing of a trapped resonantly-interacting fermion mixture with unequal spin populations. Preprint at ⟨http://arxiv.org/cond-mat/0601321⟩ (2006).
33. Clogston, A. M. Upper limit for the critical field in hard superconductors. *Phys. Rev. Lett.* **9,** 266–267 (1962).

Supplementary Information is linked to the online version of the paper at www.nature.com/nature.

Acknowledgements We thank the participants of the Aspen winter conference on strongly interacting fermions for discussions. This work was supported by the NSF, ONR and NASA.

Author Information Reprints and permissions information is available at npg.nature.com/reprintsandpermissions. The authors declare no competing financial interests. Correspondence and requests for materials should be addressed to M.W.Z. (zwierlei@mit.edu).